doi: 10.5028/jatm.v6i3.365

Direct Numerical Simulation of the Onset of Vortex Shedding for Blunt Elongated Bodies

Marcos Aurélio Ortega[1], Roberto da Mota Girardi[1], Jorge Hugo Silvestrini[2]

ABSTRACT: This research project focuses upon the wake behind a two-dimensional blunt-trailing-edged body. Data are obtained numerically by means of a Direct Numerical Simulation code. The body has an elliptical nose followed by a straight section that ends in a blunt base. The present paper is dedicated to the analysis of the onset of the shedding process. The effort is certainly worthwhile, because, in contrast to the case of the circular cylinder, the boundary layers's separation points are defined and fixed. This allows a better assessment of the vital influence of the boundary layers upon the wake, in a controlled way. This is not the case for the circular cylinder, because, in this instance, the separation points oscillate in relation to a mean position. In the present analysis, the relationship between the onset of shedding Reynolds number, Re^{h}_{K} , and the aspect ratio, *AR*, is obtained. To this end, a wide range of aspect ratios, between 3 and 25, was investigated. The result represented by this relationship is a novelty in the literature. Values of Re^{h}_{K} are strongly influenced by the aspect ratio for the case of the short cylinders — for which *AR* is low. After *AR* about 9, the curve flattens and the influence of the aspect ratio upon the shedding Reynolds number is very mild. Besides, the paper discusses another very important aspect; the overall stability of the pre-shedding laminar bubble at the base of the body. It is important to stress that the latter study relies on the fact that the boundary layers separation points are fixed.

KEYWORDS: Wakes, Onset of shedding, Blunt-trailing-edged body, Numerical analysis.

INTRODUCTION

The aim of the present work is to study the wake behind a blunt-trailing-edged body, consisting of an elliptical nose followed by a straight section (Fig. 1). In the present paper, a study of the onset of shedding is reported, whereas in a second paper, the main topological features of the flow are discussed (Ortega *et al.*, 2012).

There is a myriad of publications in the literature related to flows about blunt bodies. It is not the aim of the present authors to present here a thorough literature review about this theme. The interested reader can find these information in the following citations. Some of the most comprehensive and authoritative historical reviews are the ones by Williamson (1996) and Dauchy *et al.* (1997). On the other hand, low Reynolds number data, relative to elliptical elongated cylinders, is rather scarce. Bearman (1965) has conducted, during the 1960's, a thorough experimental analysis of this geometrical form. Two-dimensional results were presented for a model with and without splitter plates, and the Reynolds number, based on the model chord, was made to vary in the range of 1.4×10^5 to 2.56×10^5 (Bearman, 1965). Several splitter plate lengths were investigated, and studies of base pressure, shedding frequency, hot-wire traverse distributions of mean flow velocity, and r.m.s. of velocity fluctuations, were done. The main focus of the investigation was the understanding of how those factors would influence the formation length, and, at the same time, to assess the possibility of drag reduction. In a sequence, Bearman (1967), following basically the same line of study, investigated the effect of base bleed behind the same model. Now, the Reynolds number, based on the body base height, was made to vary between 1.3×10^4 and 4.1×10^4.

1.Instituto Tecnológico de Aeronáutica – São José dos Campos/SP – Brazil **2.**Pontifícia Universidade Católica do Rio Grande do Sul - Porto Alegre/RS – Brazil
Author for correspondence: Marcos Aurélio Ortega | Department of Aerodynamics – Division of Aeronautical Engineering – ITA, CEP: 12.228-001 - São José dos Campos/ SP | Brazil | Email: marcos.ts.ortega@gmail.com
Received: 04/09/2014 | **Accepted:** 06/25/2014

The model investigated had a span of 71.1 cm, a chord of 15.24 cm, and a base height, *h*, of 2.54 cm. The aspect ratio, $AR = c/h$, was equal to 6. The frontal half ellipse had semi-major and -minor axes equal to, respectively, 12.70 cm and 1.27 cm. In the words of the author: "The rear 2.54 cm of the model was parallel sided in order that the flow left the surface smoothly at the trailing edge corners". As pointed out before, this was the main geometric characteristic that attracted our attention. Recently, Park *et al.* (2006) have investigated a new passive device for drag reduction in a flow about a bluff body with a cross-section like the one in Fig. 1. The aspect ratio was equal to 6.33 and the study involved both experimental and numerical treatments. Another work that has focused on the elongated cylinder shape is the one by Ryan *et al.* (2005). In this paper, the authors conducted a numerical Floquet analysis of the three-dimensional transition to turbulence in the wake of the body.

For the case of the elongated cylinder, the onset-of-shedding process that happens at low values of the Reynolds number, the well known Hopf bifurcation, responsible for the appearance of the von Kármán vortex street, has never been investigated before. This is the main focus of this article. Values of the onset of shedding Reynolds number are numerically obtained by varying the value of the aspect ratio. For low values of the aspect ratio, the influence upon the Reynolds number in strong, but after about $AR = 9$, the curve flattens and an asymptotic behavior is observed. After that, an exploration on the influence of the boundary layers upon the shedding process was attained. For this purpose, we have "installed" small bumps on the upper and lower surfaces of the body, and have studied how those perturbations affect the conditions of the vortexes emission.

This paper is organized as follows. In the section "Computational strategy", the main aspects of the mathematical model are presented and discussed. A short review of the Hopf bifurcation is given, with the purpose of establishing the physical scenario to be tackled ahead in the study. After that, some data about validation and convergence of the code are discussed. Convergence characteristics are extremely important here because the physics is essentially time dependent. In the section "In search of the onset of shedding Reynolds number", the core of the article is divided into three sub-sections. In the first one, a strategy of investigation is designed. We have arrived at the rake of grids idea. This idea was tested, first, by dealing with the circular cylinder, taking into account the vast number of literature data for this geometry. Because the circular cylinder results were consistent, we then applied it to the elongated body. Finally, we made an effort to assess the influence of the boundary layers upon the formation and shedding of the structures at the base of the body. Some conclusions are then presented.

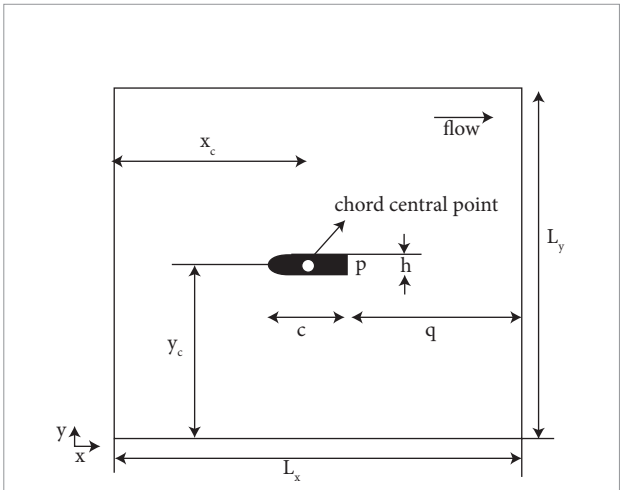

x_c, y_c = position of the body in the calculation domain, h = body base height, c = body chord length.

Figure 1. Cross-sectional view of the elongated cylinder and dimensions of computational domain.

COMPUTATIONAL STRATEGY

Firstly, solutions for flow past a circular cylinder from time-dependent simulations of the Navier-Stokes equations on two-dimensional domains are obtained. The immediate objective is to perform code convergence tests. Secondly, the code is applied to the studies of the flow about the elongated cylinder. The code is called Incompact3d and it was originally developed by Lamballais and Silvestrini (2002), and Lamballais *et al.* (2008); it is a software for incompressible flows of the immersed boundaries type and it uses compact differences for discretization purposes.

TIME DEPENDENT SIMULATIONS

We consider the flow of an incompressible Newtonian fluid. The physical behavior is mathematically modelled by the Navier-Stokes equations, written here as:

$$\vec{\nabla}.\vec{u} = 0, \tag{1}$$

$$\frac{\partial \vec{u}}{\partial t} + \vec{u}.\vec{\nabla}\vec{u} = -\frac{1}{\rho}\vec{\nabla}P + \frac{1}{Re}\nabla^2\vec{u} + \vec{f}, \tag{2}$$

where;

ρ is the density, $P(\vec{x},t)$ is the pressure field, and $\vec{u}(\vec{x},t)$ is the velocity field.

The introduction of an external force field $\vec{f}(\vec{x},t)$ is necessary, in order to simulate the presence of the body. The equations above, if written in rotational form, are stable to aliasing errors (Kravchenko and Moin, 1997); therefore, in the numerical algorithm, the following formulation is preferred:

$$\frac{\partial \vec{u}}{\partial t} = -\frac{1}{\rho}\vec{\nabla}P^* - \vec{\omega}\times\vec{u} + \frac{1}{Re}\nabla^2\vec{u} + \vec{f}, \tag{3}$$

where;

$P^*(\vec{x},t)$ is the modified pressure field (equal to $(P+\rho\vec{u}^2/2)$), and $\vec{\omega}(\vec{x},t)$ is the vorticity field (equal to $\vec{\nabla}\times\vec{u}$). The groups of equations above are written in non-dimensional form: lengths are scaled by a typical length, l_t, — the diameter for the circular cylinder, d, and the base height for the elongated cylinder, h, — and a typical velocity, which happens to be, in both instances, the magnitude of the free-stream velocity, U_∞. The Reynolds number that results from the non-dimensionalisation is given by $Re = U_\infty . l_t / \upsilon_\infty$, where υ_∞, is the free-stream kinematic viscosity.

Time-dependent simulations based on these equations in two dimensions ($\omega\equiv 0$; $\partial/\partial_z \equiv 0$) are carried out using a sixth-order, compact-finite-difference scheme (Lele, 1992). Meshes are Cartesian and the presence of the body is simulated by virtue of an immersed-boundary technique (Goldstein *et al.*, 1993). To integrate Eq. (3), a third-order low-storage Runge-Kutta strategy was used (Lamballais, 1996). The core of the algorithm solves a Poisson equation for the pressure, which, in the sequel, acts as a projector of the velocity field onto a divergence-free space (Lamballais, 1996). Part of the forcing terms in the immersed boundary sub-routine is advanced implicitly, instead, and the Crank-Nicolson scheme is used (Lamballais, 1996). This feature improves the efficiency of the forcing mechanism (Fadlun *et al.*, 2000; Lamballais and Silvestrini, 2002). All calculations presented here were performed in 64-bits precision. Further details of the code, and many verification and validation studies, can be assessed in a series of former applications, both two- and three-dimensional (Ribeiro, 2002; Vitola, 2006; Lamballais *et al.*, 2008; Silvestrini and Lamballais, 2004; Lardeau *et al.*, 2002; Laizet *et al.*, 2009). The two-dimensional approach that is used to investigate the problem is appropriate due to the fact that, when the Reynolds number is low, the flow is everywhere laminar but the main characteristics of the great structures are mostly all present (Barkley and Henderson, 1996).

Boundary conditions are required at the limits of the computational domain. At the entrance plane — left vertical boundary in Fig. 1 —, velocity components are specified according to: $u_x = U_\infty = 1$ and $u_y = 0$. A white noise might be added, in order to speed up a process of transition that is eventually being studied. At the upper and lower boundaries, the uniform flow is enforced, i.e., $u_x = 1$ and $u_y = 0$ (Ribeiro, 2002), while along the exit plane, conditions are established according to a simplified convection equation:

$$\frac{\partial u_i}{\partial t} + U_{conv}\frac{\partial u_i}{\partial x} = 0, \tag{4}$$

where U_{conv} is made equal to the main structures mean-convection velocity at the end of each iteration. The very mild degradation of the flow, imposed by this condition, is confined to a narrow region close to the boundary, according to Akselvoll and Moin (1996). The last frontier is composed of the body surface. To cope with it, following Goldstein *et al.* (1993) and Saiki and Biringen (1996), a feedback forcing term was introduced in the momentum equation, in order to represent the presence of the solid body. This procedure presents an outstanding advantage because a Cartesian grid can always be used, independently of the body's external geometry.

HOPF STABILITY ANALYSIS

For sufficiently low Reynolds numbers, the topology in the near wake of a two-dimensional bluff body is that of the laminar twin vortices. After that, and as the Reynolds number grows, an instability corresponding to a Hopf bifurcation leads to a changing of regimes. For the case of the circular cylinder, and for a Reynolds number, somewhere between 40 and 50, the steady flow field transitions to a laminar two-dimensional shedding wake, the von Kármán vortex street — Williamson (1996) reports a Re_K^d equal to 49; Dušek *et al.* (1994) inform a slightly different range, 46 - 47, while Sumer and Fredsoe (1997) give $Re_K^d = 40$. The subscript K in the Reynolds number symbol is an indicative that the value corresponds to the onset of shedding, while a superscript indicates the definition reference length. To be more specific, one should remind that, at this low

range, there are three limiting values of the Reynolds number, which we shall indicate by Re_c, Re_A, and Re_K. The subscripts correspond to "critical state", "absolute instability" and "onset of shedding", respectively. For the case of the circular cylinder and for a Reynolds number based on the diameter, Monkewitz (1988) reports the following: $Re_c \approx 5$, $Re_A \approx 25$, and $Re_K^d \approx 47$. The critical Reynolds number, Re_c, divides the ranges of complete stability ($Re < Re_c$) and convective instability ($Re_c < Re < Re_A$). Re_A marks the appearance of the first local absolute instability, while Re_K^d is indicative of the onset of vortexes shedding. See, for example, Huerre and Monkewitz (1985), or Bers (1983), or Drazin and Reid (2004), for an explanation of those stability concepts. In his studies Monkewitz investigated the stability of a family of incompressible bluff-body wakes by means of a linear parallel, that is, local, approach. One of the main results of this investigation is the confirmation that Re_K is really larger than Re_A, a result first established by Chomaz *et al.* (1988). In other words, this means that the Karman vortex street is a consequence of self-excited oscillations of the wake, and that shedding is not triggered by the first appearance of an absolute instability in the near wake. This is a necessary condition, but shedding is the "end product" of a saturated state, that is, global instability sets in after a whole region of the near wake has reached the absolute instability state (Monkewitz, 1988; Chomaz *et al.*, 1988; Yang and Zebib, 1989). Monkewitz (1988) suggests that for forms other than circular, the sequence $Re_c < Re_A < Re_K$ is maintained, but with different numerical values.

The majority of the studies which deal with the Hopf bifurcation is either experimental or analytical (based on some variation of the linearized Landau equation). There is also a hybrid approach, where the author significantly simplifies the physical scenario: by considering the basic flow as parallel, for example, and completing the study by numerical means (Triantafyllou *et al.*, 1986).

The approach to be followed in this work is the DNS, Direct Numerical Simulation, a numerical tool that solves the complete Navier-Stokes equations. The great advantage is to solve the equations in their original form, and, in doing so, to take into account the essential non-linearities of the physical problem. The disadvantage, which is also considerable, corresponds to the computer costs. The main drawback is the following. For a coarse grid, the elapsed time to reach a stable oscillating state is rather short (taking into account that the Reynolds number is already inside the shedding range). This time length is measured from the very beginning — iteration 1 —, when the field of flow corresponds to the initial state (usually, uniform distributions of parameters along the domain of calculation). The destabilizing interval of time is short, in this instance, because the numerical error is relatively large in view of the coarseness of the grid. The numerical error is the leading factor in the onset of shedding triggering process (this point will be explored further in this paper). On the other hand, if the grid is coarse, the overall accuracy will most probably be poor. Eventually then, the user might be tempted to refine the grid in order to improve accuracy. As a result of this initiative, the destabilizing interval of time will grow accordingly, because a refined grid will "offer" a smaller destabilizing effect. Because the process is truly an assymptotic one, refining the grid further will correspond to an ever increasing computational time (a similar effect can be observed in Figs. 2 and 4 in relation to compiler precision). The way we have adopted to avoid this physical/numerical difficulty is to search for pre-established ranges of Reynolds numbers, which will, at least under certain controllable circumstances, contain the true value of Re_K. That is, we will be looking for data in the form of $Re_K \pm \Delta Re$. In the sequel, the details of this strategy will be given and discussed.

CONVERGENCE TESTS

The main concern in this section is to check for approximation errors. For the cyclic flow computations, the results were verified to be mesh independent to a high degree of accuracy. These error checking studies were conducted considering the flow about a circular cylinder.

The cyclic flow calculation was submitted to a complete battery of tests. In former works, members of our team (Ribeiro, 2002; Vitola, 2006) have already investigated the "collection" of optimized code parameters — related both to domain geometry and mathematical algorithms. Notwithstanding this, and due to the nature of the present paper, we have decided to further investigate the convergence characteristics of code Incompact3d, by means of a grid-refinement study— following Barkley and Henderson (1996). To this end, we have used a $30d$ x $24d$ grid and several resolutions, as shown in Table 1. The Reynolds number was fixed in 300. Here, an enlarged grid is preferred because errors resulting, for example, from small distance of the body to the domain entrance plane and blockage effects, can be better controlled. Results are given in Table 1 showing convergence to three digits for $\Delta/d \leq 0.0167$.

Table 1. Grid refinement study of code Incompact3d.

Δ/d	$< C_d >$	C'_d	C'_l
0.0250	1.4267	0.0589	0.6776
0.0222	1.4147	0.0584	0.6703
0.0200	1.4178	0.0585	0.6718
0.0185	1.4018	0.0578	0.6615
0.0167	1.3927	0.0562	0.6483
0.0156	1.3924	0.0562	0.6482

IN SEARCH OF THE ONSET OF SHEDDING REYNOLDS NUMBER

THE STRATEGY FOR THE CIRCULAR CYLINDER

The numerical investigation in the range $Re \approx Re_K$, that is, for values of the Reynolds number in the onset of shedding region, must be done with very much care. As soon as one approaches the exact value of Re_K, the final solution gets extremely sensitive to the various parameters that have some influence in the numerical calculation. Basically, every factor has its influence in the final shedding conditions: (i) Grid resolution (probably, the most influential one); (ii) Type of numerical algorithm; (iii) Domain overall sizes (L_x and L_y); (iv) Accuracy — if single or double precision; (v) Time step; (vi) Type of machine: if 32 or 64 bits; (vii) For codes of the immersed boundary type — as the one here employed is —, how smoothly is the perimeter of the body represented. These items bring to the stage the question of the computational error, a factor that helps to trigger the shedding process when it grows up to a certain point. The problem of the blockage comes embedded in item (iii), and is especially related to L_y. Item (iii) also includes the effect of the position of the body in relation to the domain boundaries, especially the entrance plane. The time step has an indirect effect, because as the grid is refined, most probably one will be required to lower it, in order to guarantee convergence. The Reynolds number is evidently a prime influence. Besides all those aspects, there is still to be remembered the fact that the closing-in process to Re_K is, in a way, always asymptotic, and, most certainly, the investigation will require running the code for long intervals of time. In the sequence, we will return to some of these points and discuss them further.

After some work, we devised what was judged as a good approach to the problem. The core of our strategy corresponded to the creation of a sort of a "grid rake". This means a collection of grids with different resolutions. The testing of the idea was done considering the flow about a circular cylinder. For this specific case, five meshes were used in the study, corresponding to $[n_x/d] = [n_y/d] = 12$, 18, 24, 30 and 36, where d stands for the circular cylinder diameter. The domain of calculation dimensions were adopted as $L_x = 19d$, $L_y = 12d$, and $x_c = 8d$ (these values are the results of optimizing studies by Ribeiro (2002); for a Reynolds number equal to 300, these studies indicate $n/d = 24$ as a best value for the number of grid nodes per diameter).

The fact is that, the numerical investigation of the onset of shedding neighborhood is difficult, time consuming, and very elusive. Therefore, we concentrated mainly on the grid resolution, and probed other influences more superficially. The main aim of this particular effort is to try to develop a viable and reliable criterion that could be applied to the Re_K region, especially now to the elongated cylinder studies.

We studied the flow about the circular cylinder in the range of Reynolds number from 40 to 50. Table 2 shows the wake flow state for the various cases investigated. The first column of the table gives the value of the Reynolds number, while the first line indicates the grid resolution in terms of grid points per cylinder diameter. We began by running the case $Re = 40$ and ended with $Re = 50$, and the intermediate values are shown in Table 2. Each of these values of the Reynolds number was investigated using the five grid resolutions, as shown in Table 2, $[n_x/d] = [n_y/d] = 12$, 18, 24, 30, 36. All cases were run in single precision in a 64-bits machine, and at least from t = 0 up to t = 1000 units of non-dimensional time. The dimensionless time step was always the same and equal to 0.004838, which corresponded to a safe value that would guarantee the convergence at the finer grids. For $Re = 40$, 41 and 42, there was no shedding, and the signal of the anemometers indicated damping (some "numerical" anemometers were strategically placed in certain positions along the grid.) When the Reynolds number was raised to 43 there was shedding for resolution 12/d. The first Reynolds number value for which we obtained vortexes shedding in all grids was $Re = 45$. One would be then tempted to define 45 as the value of Re_K^d for the cylinder, but there is a crucial point here. We do believe that it is basically not possible to define an absolute value of the onset of shedding Reynolds number,

Table 2. Condition of the circular cylinder wake in the onset of shedding range.

Re^d	12/*d*	18/*d*	24/*d*	30/*d*	36/*d*	36/*d* (0.01%)	36/*d* (0.1%)
50	s	s	s	s	s	–	–
47	s	s	s	s	s	–	–
45	s	s	s	s	s	–	–
44	s	s	s	d	d	s	s
43	s	d	s	d	d	d	s
42	d	d	d	d	d	d	d
41	d	d	d	d	d	–	–
40	d	d	d	d	d	–	–

s: vortexes shedding; d: vortexes damping (Calculations performed in single precision).

at least when one is using an experimental or numerical tool to probe the process. The most one can do is to search for a range of values inside which one can probably guarantee, under certain controlled conditions, that the value of Re_K^d resides.

To clarify this point, let us focus our attention upon the case "43/18d", in Table 2. In this instance, there was no shedding until $t = 1000$. On the other hand, how can one be sure that the shedding will not set in for a certain instant of time after that limit? As we have stressed before, the final stability of the laminar bubble system in the wakeside of the cylinder is a characteristic of the system *perse*. In other words, given the state of the final saturation, the onset of shedding settles in. Therefore, what might be happenning here is that, for $t = 1000$, we have not yet reached the final saturated state. If this is the case, running for a longer stretch of time would almost inevitably result in shedding due to the mounting of the overall instability, which is ultimately fed by the numerical errors, being introduced in every iteration. Putting it differently, the result in Table 2 for the 43/18 case is conditioned to the length of the pre-defined time interval, equal, in this case, to 1,000 units. To be really sure, one would have to run the case for a much longer time stretch. If the setting 43/18 is physically not a shedding case, the feeding of perturbation at each iteration would never saturate the laminar bubble system, and the machine would run indefinitely without disturbing the damping state. This is why we argue that, for numerical, as well as for experimental investigations, it is not possible to fix an absolute value of the shedding Reynolds number. In this work, we will concentrate on the effort of determining the ranges of Re_K.

A careful observation of Table 2 reveals an unexpected result relative to $Re = 43$. Because the arrangement 43/18 corresponds to a damped flow, with more reason, the combination 43/24 should also correspond to a damped case. In normal conditions, the amplitude of the numerical error distribution along the grid is the main drive for the shed triggering. All combinations in Table 2 were run in a 64-bits machine (Dell Precision 690) with single precision. In any case, the amplitude of the error diminishes as the grid is refined. After some investigation we found out that the 24 points per diameter grid does not match as best as possible, as it should, the cylinder perimeter. That is, for this resolution, some nodes get slightly mispositioned along the perimeter. This "mispositioning" is recognized considering the details of the immersed boundary strategy. In practice what happens is that the flow in the numerical calculation "sees", in this case, the cylinder as a body with an augmented rugosity in its surface. Therefore, the perturbation increased, since 43 is located in a very critical position in relation to the interval that is being investigated ($Re = 40$ - 45), i.e., exactly at the centre of the stretch, the case 43/24 came out of the calculation as a shedding case and not as a damped one.

Because the points previously stressed are too important, we would like to illustrate them further. A clear evidence of the fact that the error amplitude is decisive is given in Fig. 2. We rerun several 12 points per diameter cases, but now using double precision, and a much longer calculation that reached 10 141.26 units of time. The running of the code, for such long stretches of time, can be looked at as a severe test for the damping characteristic of the flow. Besides, one has to keep

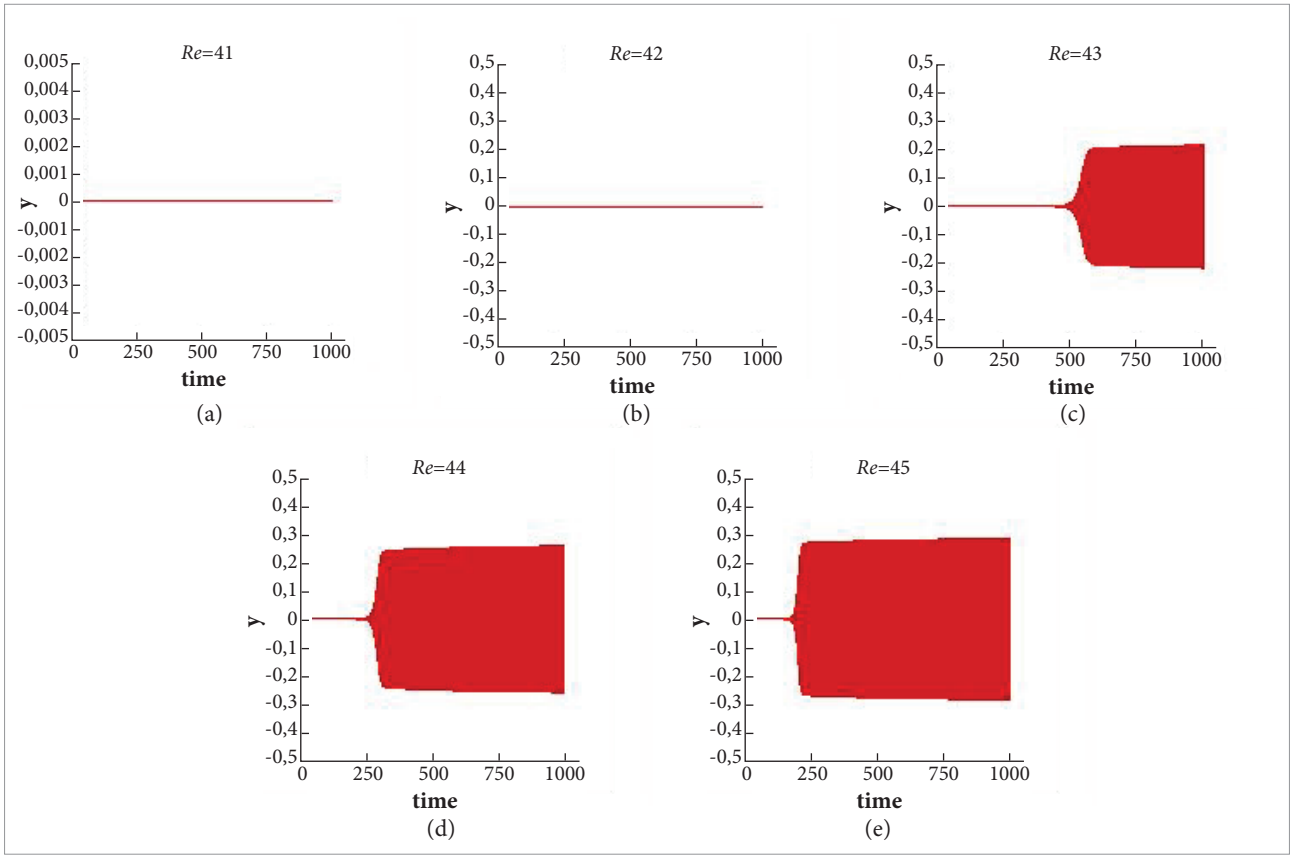

Figure 2. History of the crosswise velocity component, υ, for the circular cylinder and several values of *Re*. Grid resolution=12/*d*. Processing in double precision

in mind that we are using here the coarser grid, the one that rises the largest amount of error. The reader can perceive that shedding was damped for *Re* = 41 and *Re* = 42, and very much delayed for the other cases. The reason is evidently the fact that the truncation error has decreased when the compiling precision was increased. As a final test following this line, we introduced a white noise with amplitude of 0.0001, with the basic aim of speeding the onset of shedding. The results are shown on Fig. 3, and when compared with Fig. 2, they confirm the expected speeding of the process. When submitted to this level of excitation, the *Re* = 42 case did not "resist" and the shedding was initiated, only after about 7,500 units of time. Besides, and again from Fig. 3, one can appreciate the fact that the introduction of this level of noise corresponds basically to running the cases in single precision — compare it to Fig. 4. In fact, and the reader should keep this in mind, what is happening here is that for this grid resolution and double precision compiling, the beginning of vortexes emission was delayed, but not eliminated. The introduction of the white noise simply "pulled" the shedding process back to an earlier time, what evidently spares a lot of computing time. On the other hand this is a clear example of the difficulties associated to the study of transitional physical problems. The last word about a certain case, i.e., if the flow has finally reached the final global response — Kármán vortex shedding, Monkewitz (1988) —, or not, depends upon many factors, and much care must be exercised.

Attention was also paid to the other side of Table 2. Flows with Reynolds numbers 42, 43, and 44 were simulated again, but now subjected to higher levels of excitation. This was accomplished by raising the white noise amplitude. Columns "36/*d*(0.01%)" and "36/*d*(0.1%)" contain results for the 36-nodes-per-diameter grid and levels of perturbation of 0.01% and 0.1%, respectively. Again we observe that shedding was obtained for some Reynolds numbers that, otherwise, when excitation was smaller, corresponded to damped cases, at least during the length of time of numerical simulation — 1,000 units. Another clear evidence from Table 2 is the very

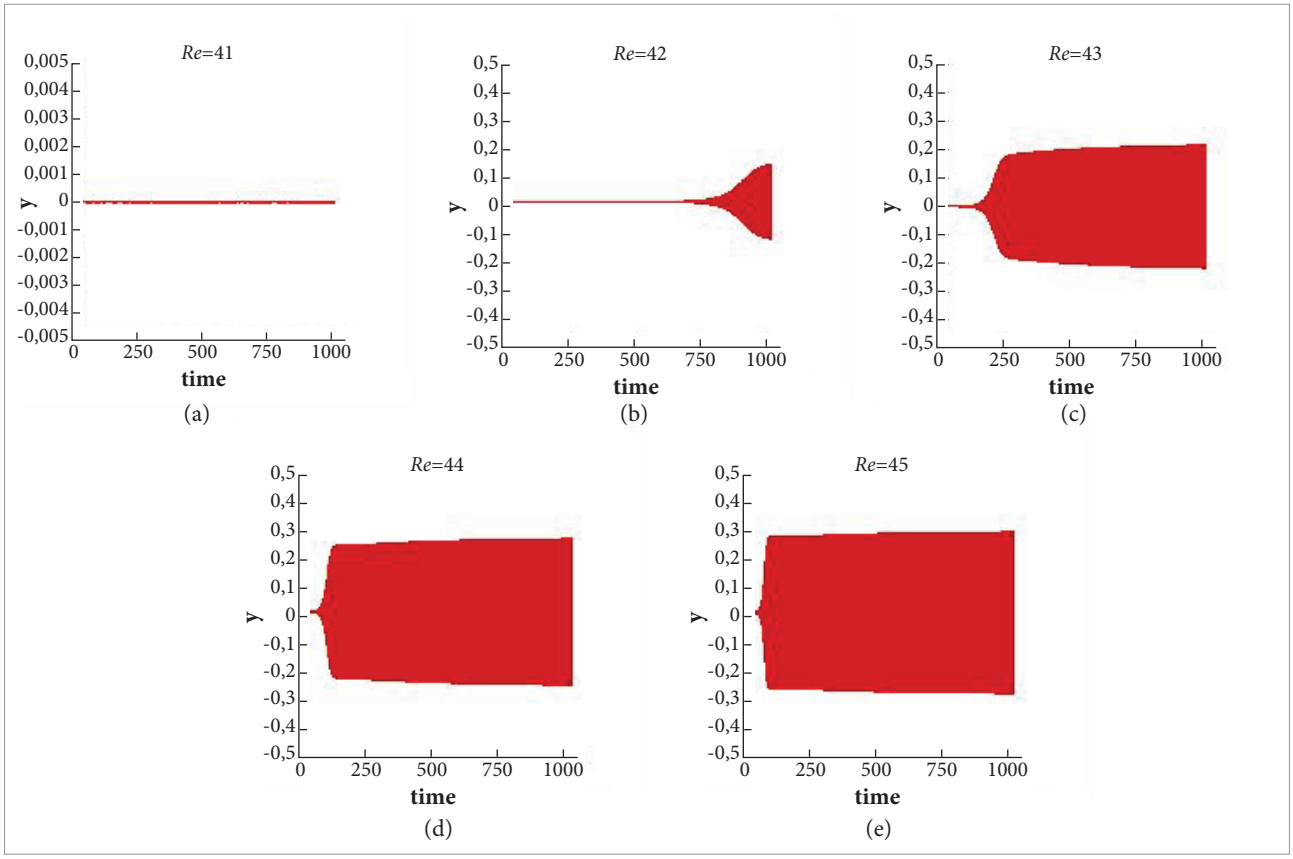

Figure 3. History of the crosswise velocity component, υ, for the circular cylinder and several values of *Re*. Grid resolution=12/*d*. Processing in double precision and a 0.0001 amplitude white noise.

important fact that studies of onset of shedding, as well as every investigation on transitional phenomena, being it experimental or numerical, must bring clearly the information relative to the levels of turbulence/perturbation under which the experience was carried out. Otherwise, an isolated figure, in this specific case the value of the Reynolds number, carries the risk of getting almost meaningless. Maybe the only thing that can be assured is that the provided number furnished falls inside a very wide interval generally well established in the literature.

If one compares all those results carefully, and takes into account the arguments previously presented, it is possible to state that the "scanning" of the Reynolds number interval by a rake of grids in single precision and a relatively "small" time stretch (about 1,000 units) is a guarantee that the interval is well located, at least, say, to "first order". The error of the code in single precision (that corresponds, for the present code, to a perturbation level of 0.01% — compare Figs. 3 and 4) is capable of triggering the shedding process according to the right trends. That is, if we use, for example, double precision, what happens is that the shedding, in most cases, will be delayed, but, most certainly, not eliminated. We believe that, under those circumstances, and restrained by the conditions of the numerical simulation — among which the most influential is the grid refinement —, it is possible to state, after Table 2, that the onset of the shedding Reynolds number is located in the interval $Re_K^d = 43.5 \pm 1.5$. If one decides to reach a second order level of accuracy in the determination of Re_K, then the computational cost will be amplified by many folds. For example, to run a 36-points-per-diameter case in double precision, and reach 10 ,000 units of time, one would need about 2,100,000 iterations, what, in the case of our Dell Station 690, took about 40 (forty) days of calculation. This is because the largest time step for guaranteeing convergence is equal to 0.00483786, due to the grid spacing. For reasons of our convenience, the investigation

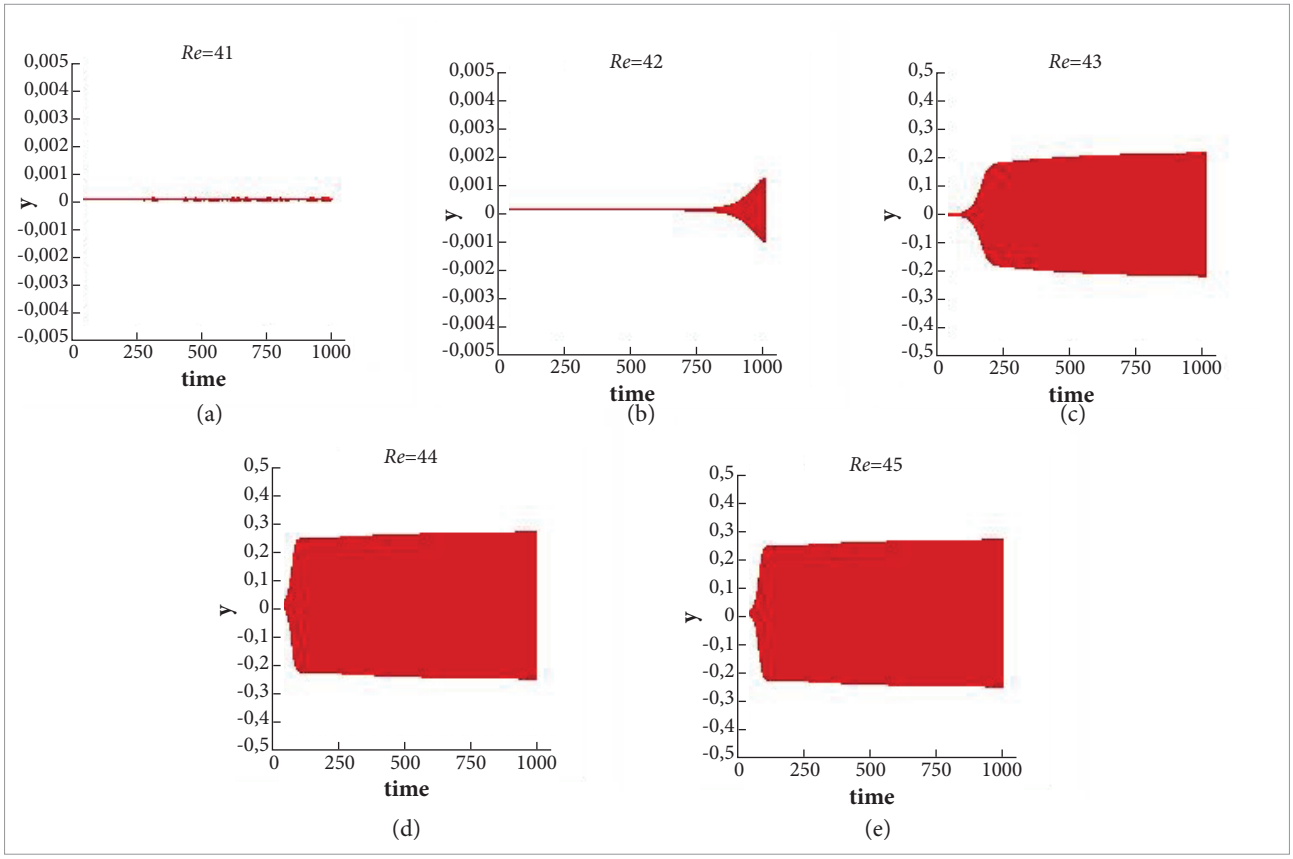

Figure 4. History of the crosswise velocity component, υ, for the circular cylinder and several values of *Re*. Grid resolution=12/d. Processing in single precision.

that is being reported here was performed using the serial version of code Incompact3d.

THE ELONGATED CYLINDER ONSET OF SHEDDING STUDY

The objective of this section is to apply to the elongated cylinder the technique that was established for the case of the circular cylinder. Before going into the details, it is important to describe how the different aspect ratios were investigated. The immediate idea would be to maintain the body base height fixed and to adapt the chord length to the desired aspect ratio. It is obvious that, in doing so, the domain of calculation total length, L_x, would increase according to the increase of the aspect ratio. Therefore, having in mind the goal of sparing grid nodes, we decided differently: to keep the chord fixed and to diminish the base height. In both cases, however, either keeping the chord length or the base height fixed, one has to care about the similarity of both the overall size of the domain of calculation and the grid resolution. This is essential in order to obtain results that can be compared on the same basis. Observe Fig. 1. The following rules were then established: (i) The ratio $L_y=h$ was kept constant; this would assure that any blockage effect, whatever its extension, would, in principle, be the same for every configuration and for every code run. (ii) The ratio $q=h$ was also kept constant; therefore, the influence of the exit plane would be felt in the same terms in every running of the code. By keeping constant the ratios $L_y=h$ and $q=h$, the same similar evolution domain was offered to the wake, irrespective of the actual investigation. (iii) The ratio of grid nodes per base height, n^h_y/h, where n^h_y is the number of crosswise grid points, allocated at the body base height, was kept the same from case to case. This figure ultimately defines n_y the total number of points along L_y.

The rake of grids for this study was composed of three choices whose number of points were: $[n^h_y/h]$ = 12, 20 and 30. It is more difficult to select the grids and the resolution in

the case of the elongated body when compared to the circular cylinder. The difficulties come from the geometric constraints, to guarantee similarity, plus the fact that the total number of grid nodes for each direction has to be a product of the form $[2^a3^b5^c]$, in order to meet the "needs" of the fast Fourier subroutines. Table 3 shows the main grid characteristics of some of the cases.

The result of the investigation is plotted in Fig. 5. It is important to draw attention to the fact that each point in this figure is the result of a rather long process. Many Reynolds number values had to be tried, and for each of them, the extension of the time of calculation was about 1,000 units of non-dimensional time, which demanded a large number of iterations (generally, on the order of six digits). Only after that, one can be sure that the onset of shedding for that particular case was attained. A minimum number of at least 100 steady cycles of emission was made to run, before guaranteeing that the case corresponded to a real "onset of shedding" case. The calculations were performed in a 64-bits machine (Dell Precision 690), and the Fortran compiler was the Intel ifort version running in single precision. In Fig. 5, the vertical

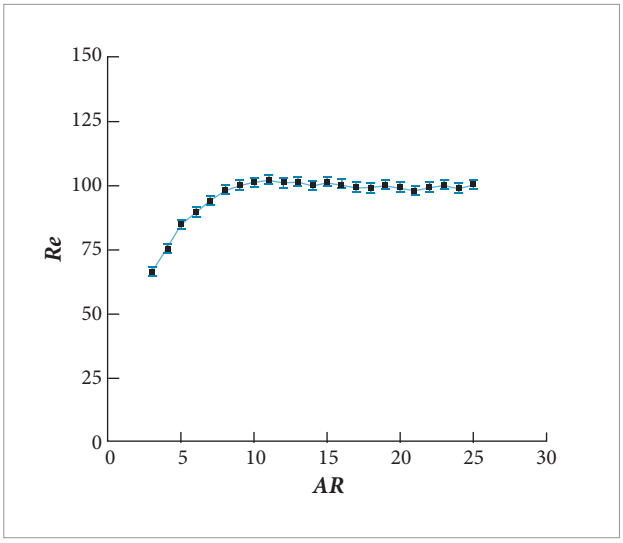

Figure 5. The dependence of Re^h_K on the elongated cylinder aspect ratio, *AR*.

Table 3. Data relative to the principal domains and grids that were used in the study of the elongated body onset of shedding. Observe that lengths are given in base heigths.

AR	n^h_y/h	$L_x=h$	$L_y=h$	n_x	n_y	x_c/h	q/h
3	12	30.0	15.0	451	181	13.5	15.0
	20	30.0	15.0	601	301	13.5	15.0
	30	30.0	15.0	751	451	13.5	15.0
7	12	45.0	15.0	481	181	26.5	15.0
	20	45.0	15.0	751	301	26.5	15.0
	30	45.0	15.0	901	451	26.5	15.0
12	12	45.0	15.0	541	181	24.0	15.0
	20	45.0	15.0	601	301	24.0	15.0
	30	45.0	15.0	901	451	24.0	15.0
18	12	60.0	15.0	541	181	36.0	15.0
	20	60.0	15.0	601	301	36.0	15.0
	30	60.0	15.0	901	451	36.0	15.0
25	12	75.0	15.0	601	181	50.0	15.0
	20	75.0	15.0	601	301	50.0	15.0
	30	75.0	15.0	901	451	50.0	15.0

bar for each point is an indication of the spreading extension of the Reynolds number as function of the grid resolution. For example, for AR = 14, the result is Re^{h}_{K} = 100 ± 2.0. Therefore, taking into account the envelope of restrictions of the numerical prediction — that we have tried to point out during the discussion so far —, it is guaranteed that the true value of Re^{h}_{K} falls inside the spreading interval defined by the vertical lines. On the other hand there is a lot of other factors that might influence this spreading range, as we have discussed previously in the case of the cylinder. However, the grid resolution is indeed the main factor. We do believe that these data (especially, Fig. 5) are important, and have not as yet been published in the literature.

Two important results stem immediately as one observes Fig. 5. Firstly, the Reynolds number grows almost linearly for small values of the aspect ratio, and after an AR equal to 9 it behaves in a plateau-like fashion, leveling at about 100. Ryan *et al*. (2005), in the context of a three-dimensional investigation, have already called attention to the increase in the onset-of-shedding Reynolds number with aspect ratio. Secondly, because the functional relationship of Re and AR is practically linear in the range 3 to 6, an extrapolation of this line to values of AR less than 3 would meet a vertical line through AR = 1 in a range of Reynolds numbers between 45 to 50. It is exactly in this region that the circular cylinder critical Reynolds number is located. It is important to remind that the circular cylinder has an aspect ratio equal to 1.

In the present two-dimensional study we learn that, for small values of AR, the Reynolds number really increases, but afterwards it levels off to an almost constant value (at least, up to AR = 25). The main reason for this behavior is suggested by Fig. 6. Instant vorticity fields are shown where values are made dimensionless regarding U_{∞} and h. Following the order (a), (b), (c), and (d), for $[n^{h}_{y}/h]$ = 12, one may appreciate, respectively, snapshots of cases AR = 3, Re^{h}_{K} = 66.5, t = 1930.31 (units of non-dimensional time); AR = 6, Re^{h}_{K} = 89.5, t = 758.33; AR = 9, Re^{h}_{K} = 100.0, t = 1004.09 and AR = 12, Re^{h}_{K} = 101.0, t = 1011.41. The flow about the body and especially the boundary layers asymptote to a common pattern, what Ryan *et al.* (2005) called a "near-universal" boundary layer. Putting it differently, for low values of AR, the boundary layers are still carrying the history of their initial formation at the ogival front part. As the aspect ratio increases, the flow, especially that part near the tip of the body base, just before separation, gradually looses the influence of the ogive and behaves more like a flow along a flat plate. This is apparent for cases (c) and (d), AR = 9 and 12, where the physical scenario of the streams along the walls of the bodies is exactly alike.

THE INFLUENCE OF THE BOUNDARY LAYERS

In this section, we will investigate the possible influences of the boundary layers "running" above and below the body upon the physical scenario at the body base and near wake. The main interest at this point is to investigate some specific influences of the boundary layers upon the onset of shedding condition. One should pay special attention to this point. The present study is made possible due to the special geometry of the elongated cylinder. The presence of the two flat surfaces that constitute the body, plus the fact that the separation points are fixed, are instrumental. It is not possible to repeat the same numerical experiments with the circular cylinder, because of the everlasting excursions of the separation points during the shedding state.

The first aspect to stress is that the boundary layers at the tips of the body base, just before separation and at the onset of shedding state, are always laminar. The reader can find, in Fig. 7, data about the layers thicknesses and shape factor as functions of the aspect ratios. For each point in the figure, the Reynolds number corresponds to Re^{h}_{K}, the onset of shedding value. By the value of H, the shape factor, one can see that the boundary layers are laminar. One should remind that, for the laminar boundary layer along a flat plate and without pressure gradient H is equal to 2.59 (Schlichting, 1979). At this point of this research project, we are focused upon the low Reynolds number range, for which the boundary layers and, most of the time also the shear layers, are laminar. One can find in the literature some studies related to the influence of the turbulent boundary layers upon the characteristics of the wake — Sieverding and Heinemann (1990); Rowe *et al.* (2001) —, but in general the Reynolds numbers are much larger (the works are mostly experimental) and the emphasis lies on the analysis of "macro" parameters, for example, the influence of the boundary layer shape factor upon the shedding frequency, and studies alike. In Fig. 8, for AR = 7 and Re^{h} = 95, we have plotted the boundary layers profiles at the upper and lower tips of the body base, for eleven instants of time of a complete cycle of emission. Precisely in the case of Fig. 8, the cycle starts at t = 288.88 and ends at t = 290.12. Plotted in the figure, there are eleven profiles for the upper tip and

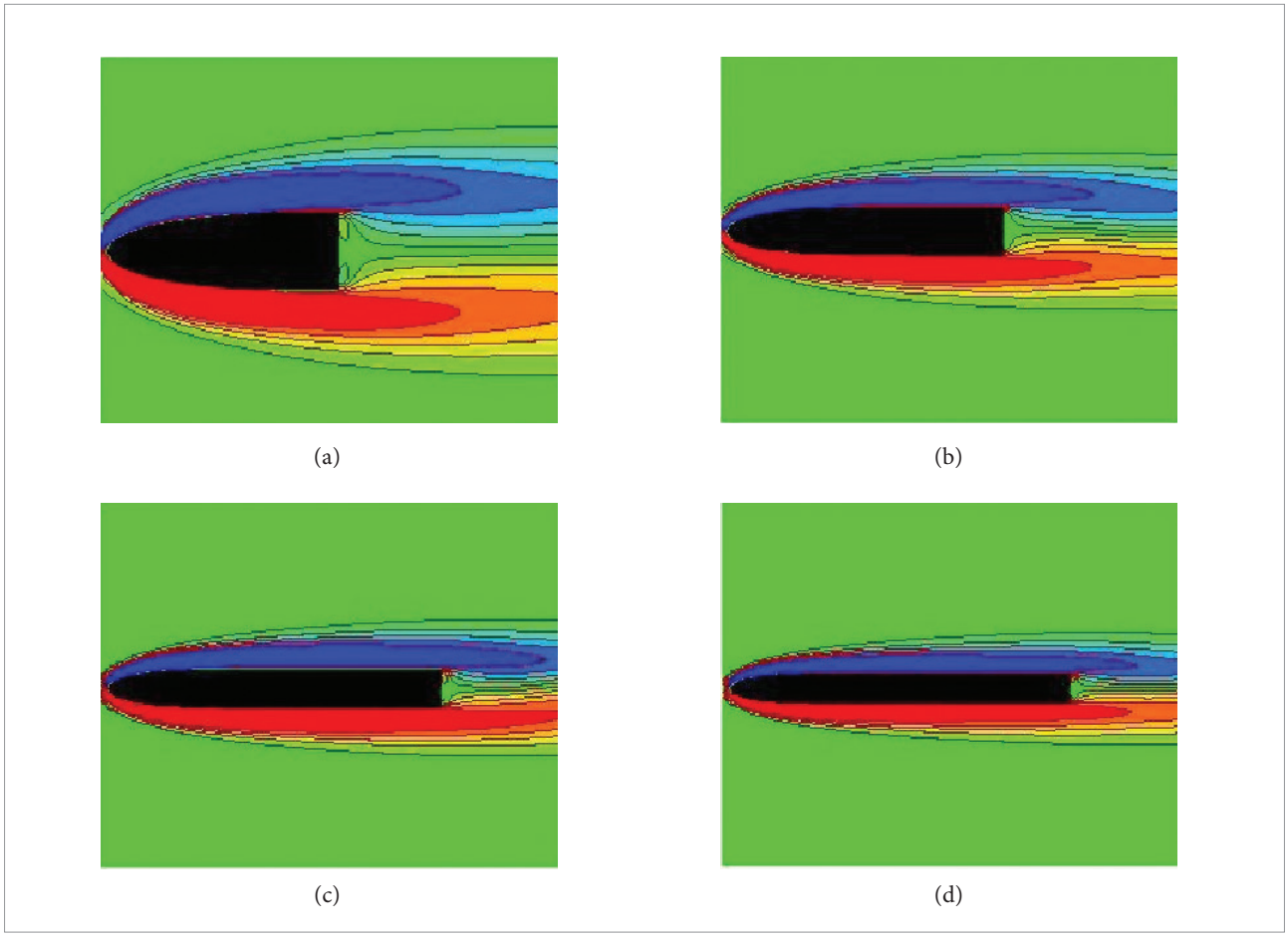

Figure 6. Instant vorticity fields at the onset of shedding *Re*. (a) $AR = 3$, $Re^h_K = 66.5$, $t = 1930.31$, $-1.33 \leq \omega_z \leq 1.33$, $\Delta\omega_z = 0.27$; (b) $AR = 6$, $Re^h_K = 89.5$, $t = 758.33$, $-1.17 \leq \omega_z \leq 1.17$, $\Delta\omega_z = 0.23$; (c) $AR = 9$, $Re^h_K = 100.0$, $t = 1004.09$, $-1.0 \leq \omega_z \leq 1.0$, $\Delta\omega_z = 0.2$; (d) $AR = 12$, $Re^h_K = 101.0$, $t = 1011.41$, $-1.0 \leq \omega_z \leq 1.0$, $\Delta\omega_z = 0.2$.

eleven for the lower one (the cycle was divided in ten equal time intervals). The case is that, the eleven profiles are basically coincident in the scale of the figure, and it seems that there is only one plotted distribution of the horizontal velocity component. What one can learn from this figure is that, in a situation where there is already vortex shedding — let us remind that for $AR = 7$ the onset of shedding Reynolds number is 94.0 —, there is virtually no variation in the boundary layers profiles during a whole cycle of emission. If we invert the argument, one may verify that, if the profiles do not change with time during a whole cycle, most probably they do not have any influence upon the mechanism of vortex liberation in the formation region. This is another indication that the global instability with the consequent vortexes evolution and shedding is a specific characteristic of the wake itself, considered as a dynamical system.

Because this is a point of paramount importance, we have focused onto it and introduced new numerical experiments. Using the geometries corresponding to $AR = 6$, 14 and 22, the following extra cases were investigated. The body shapes were slightly changed by introducing two small bumps, one at the upper wall, and another at the lower one. The bumps were made triangular, with heights equal to $1.0dy$, $0.5dy$ and $0.25dy$; the bases of the triangles were always equal to $2dx$. The position of both bumps were defined at half-base height, one base height and two base heights, upstream of the upper and lower tips of the trailing edge. The $12/h$ grid and single precision were used again in those experiences. In this part of the investigation, for every situation, we mostly used the

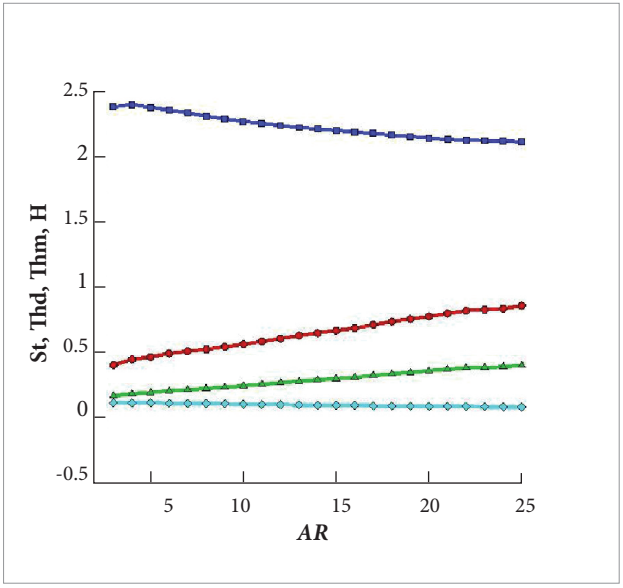

Figure 7. Strouhal number, tip boundary layers thicknesses and shape factor at the onset of shedding *Re* as function of the aspect ratio. The reference length is always the base height, *h*. *St*: Strouhal number (diamonds); T_{hd}: displacement thickness (circles); T_{hm}: moment thickness (deltas); *H*: shape factor (squares).

value of $Re^{h}=(Re_K^{h,12} - 1)$, that is, the onset of shedding Reynolds number for that configuration and the grid resolution equal to 12/*h*, minus one unity. The main final results are presented in Table 4 and Fig. 10. In Table 4, the crossing of a row and a column corresponds to one case studied; for example, "14" and "*h*/0.5*dy*" indicate an *AR* equal to 14, and both bumps, the upper and the lower ones, positioned one base height upstream of the base tips, being the height of the bumps equal to 0.5*dy*.

Details of the top tip boundary layers are depicted in Fig. 10. In pictures (a), (b), and (c), the reader can observe four lines marked with symbols: squares, circles, deltas and right triangles, corresponding, respectively, to the plain body, bumps at 0.5*h*/0.5*dy*, bumps at 1*h*/1*dy*, and bumps at 2*h*/1*dy*. There are some important aspects about those profiles. The bumps introduce a distortion in the boundary layer profile in the form of a retracting defect, situated approximately between 0.1*h* and 0.6*h* from the wall. Figure 10 depicts details of those regions for a better understanding of the point. When plotted together in a normal scale, it is practically impossible to detect those differences in the value of the horizontal velocity component. Even in the extended scale of Fig. 10, it is not possible to differentiate between the plain body and the (0.5*h*/0.5*dy*)-bumps cases. The square and circle symbols, and their corresponding lines, are coincident. For the other instances, i.e., bumps at 1*h*/1*dy* and 2*h*/1*dy*, the defects in the values of the velocity in relation to the plain body distribution, and for a distance of the wall of $y/h = 0.25$, are 0.035/0.02 ($AR = 6$), 0.02/0.01 ($AR = 14$) and 0.015/0.005 ($AR = 22$), respectively. Hence, the influence of the bumps upon the tips' boundary layers diminishes as the aspect ratio grows. By "tip" we mean the point that belongs at the same time to the flat plate and to the base of the body. By observing Fig. 9, one can grasp why this is so. As the aspect ratio grows the thickness of the boundary layers along the walls of the body also grows. Therefore, for larger values of *AR*, the perturbation due to the bumps has to evolve in a region of the boundary layer relatively closer to the wall, and where shear stresses are larger. This is an indication that the perturbation signal will be more dissipated until reaching the base tip. And the dissipation will be larger for larger values of the aspect ratios. This is probably the reason why there was no shedding for $AR = 22$ (Table 4).

The fact that stems from Fig. 10 and Table 4 is that we only had shedding for a value of the Reynolds number equal to $(Re_K^{h,12} - 1)$ when the perturbation amplitude grew beyond a certain level. Based on these results, one might appreciate a very important aspect of a bluff body wake. Given that the level of disturbances is sufficiently low (in the "linear" range, say), the "command" of the onset of shedding state is dictated by the wake itself. Only after sufficiently raising the level of the amplitude of the perturbation (the "non-linear" range, say), is that it is possible to disturb, from upstream, the overall state of the twin bubbles at the body's base region. This agrees with many previous studies, e.g., to name a few, Monkewitz (1988), and Yang and Zebib (1989), for the case of the circular cylinder, and Jackson (1987) for an assortment of geometrical forms. See also Mathis *et al.* (1984) and Provansal *et al.* (1987), who report important experimental studies about the Karman instability for the circular cylinder. The reader should appreciate how important this result is. In the case of the elongated cylinder, because the points of separation are fixed, one may conclude, apparently with no possible doubt, that the wake is unstable by itself; for the circular cylinder, even if the boundary layer profiles did not vary during a whole cycle, the oscillation of the separation points — which would prevent a definitive affirmation — is

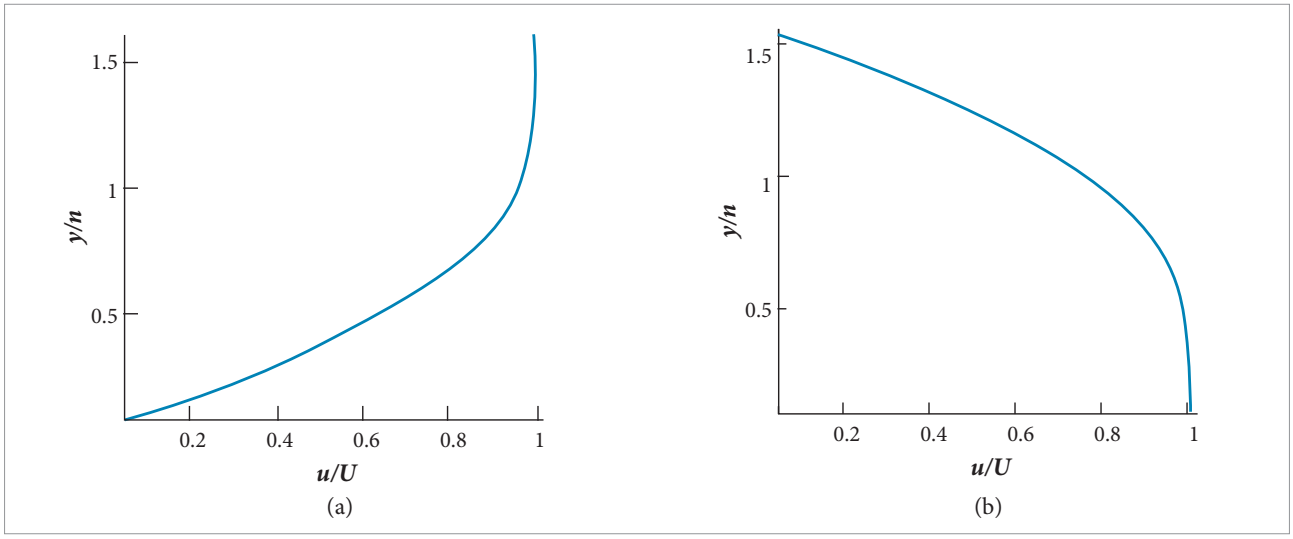

Re^h = 95; AR = 7.

Figure 8. Comparison of boundary layer profiles along a shedding cycle: (a) upper tip; (b) lower tip.

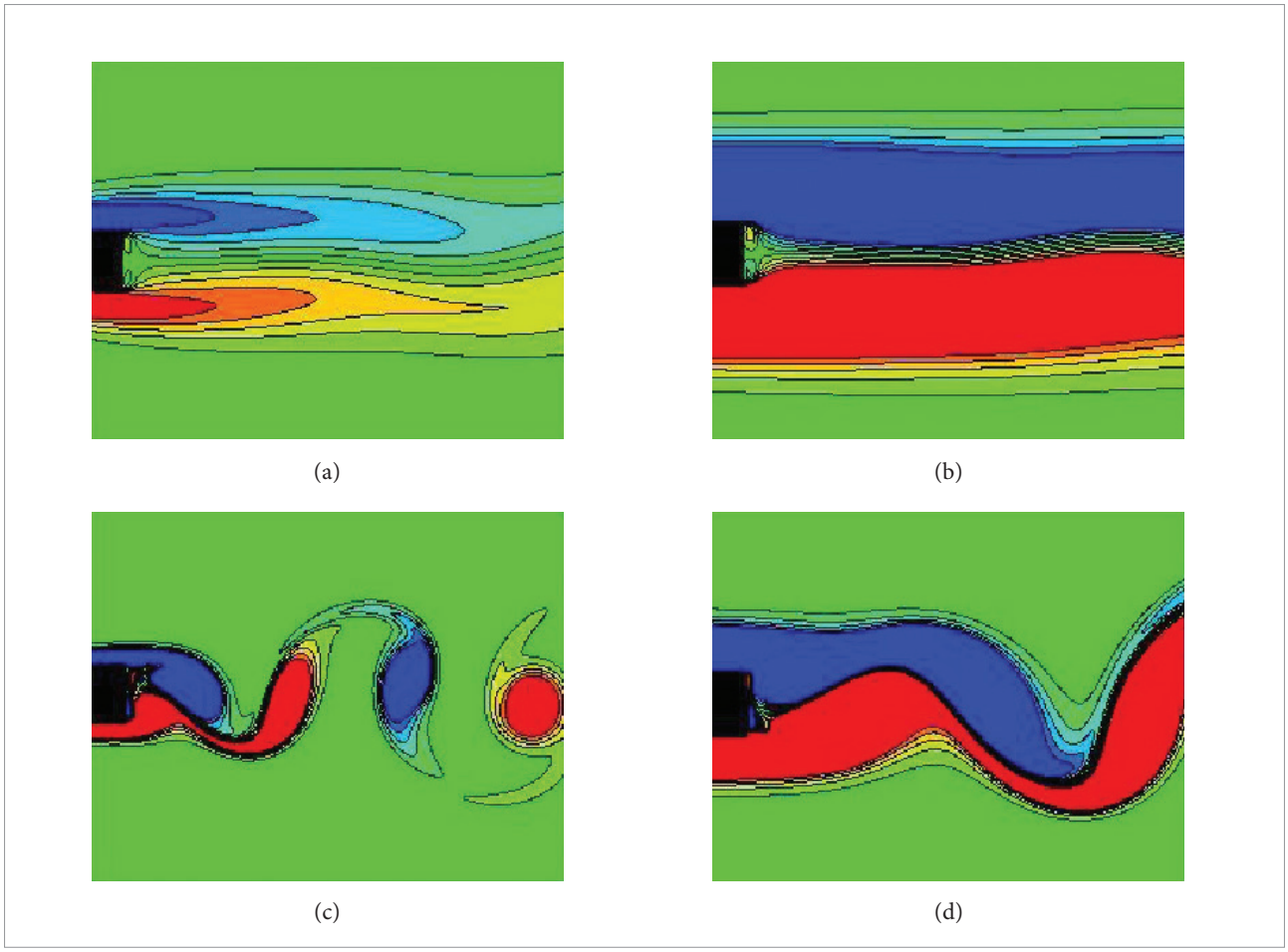

Figure 9. Instant vorticity fields at different aspect ratios: (a) AR = 3, Re^h_K = 66.5, t = 1930.31; (b) AR = 3, Re^h = 300, t = 112.28; (c) AR = 12, Re^h_K = 101.0, t = 1008.39; (d) AR = 12, Re^h = 300, t = 35.81.

Table 4. Investigation of upstream influences upon the flow about some representative aspect-ratio geometries. The Reynolds number is one unity less than the onset of shedding Reynolds number for each geometry (and a grid resolution equal to 12/*h*).

AR	Re^h	$_{Re}h,12$	0.5h/0.5dy	*h*/dy	*h*/0.5dy	2*h*/dy
6	87	88	ns	s	ns	ns
14	97	98	ns	s	ns	ns
22	96	97	ns	ns	ns	ns

s: shedding state; ns: no shedding.

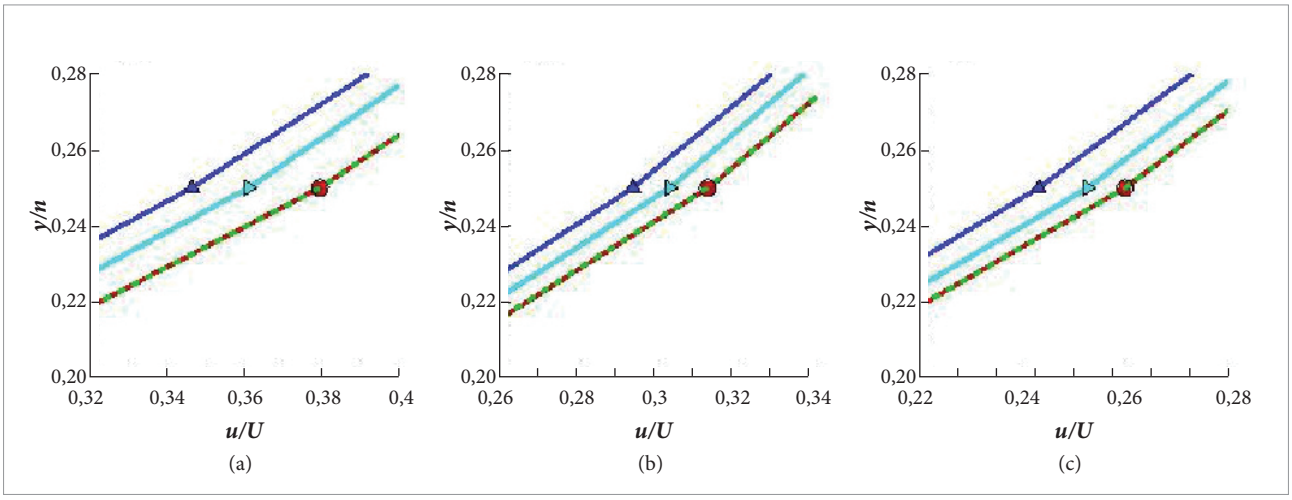

Figure 10. Details of tip boundary layer profiles. (a) *AR* = 6 and Re^h = 87; (b) *AR* = 14 and Re^h = 97; (c) *AR* = 22 and Re^h = 96. The symbols indicate: Squares: no bumps; Circles: bumps at 0.5*h*, height 0.5*h*; Deltas: bumps at 1*h*, height 1.0 d_y; Right triangles: bumps at 2*h*, height 1.0 d_y.

still to be considered. The reader should also be aware that we are not trying to state that for the case of the circular cylinder the wake is not unstable by itself, but that it may depend on the oscillation of the separation points. There are sufficient arguments in the literature to sustain the point that, for the circular cylinder, the wake is also self unstable. What we are trying to convey is the fact that the case of the elongated cylinder, for which the separation points are fixed, helps to better clarify and fix the point.

For the range of Reynolds number we have focused on, the boundary layers work as "conveyors" of vorticity, feeding the bubbles at the base region. This may be observed in Fig. 11. The instant bubbles are shown for the *AR* = 14 configuration and for several Reynolds numbers. For each frame we call attention to the value of the vorticity at certain specific points. The points at the separation stations correspond to the maxima of the vorticity at the tip boundary layer transversal section. The points located inside the bubble correspond to the approximate bubble centre, and the values on top of the upper bubble are located one base height from the vertical wall. As the Reynolds number grows towards the onset of shedding state the overall level of vorticity grows at the base region. It is evident that, with the raising of the vorticity, the length of the bubbles grows and the state of instability saturation is finally reached.

The numerical experiments represented in Fig. 5 and the data collected seems to indicate that the boundary layers feed vorticity, but the transition of the wake to another state of flow — the crossing by the point of bifurcation —, is determined by the dynamics of the bubble itself. On the other hand it is evident that much more work is needed, especially stability studies, in order to better support these conclusions.

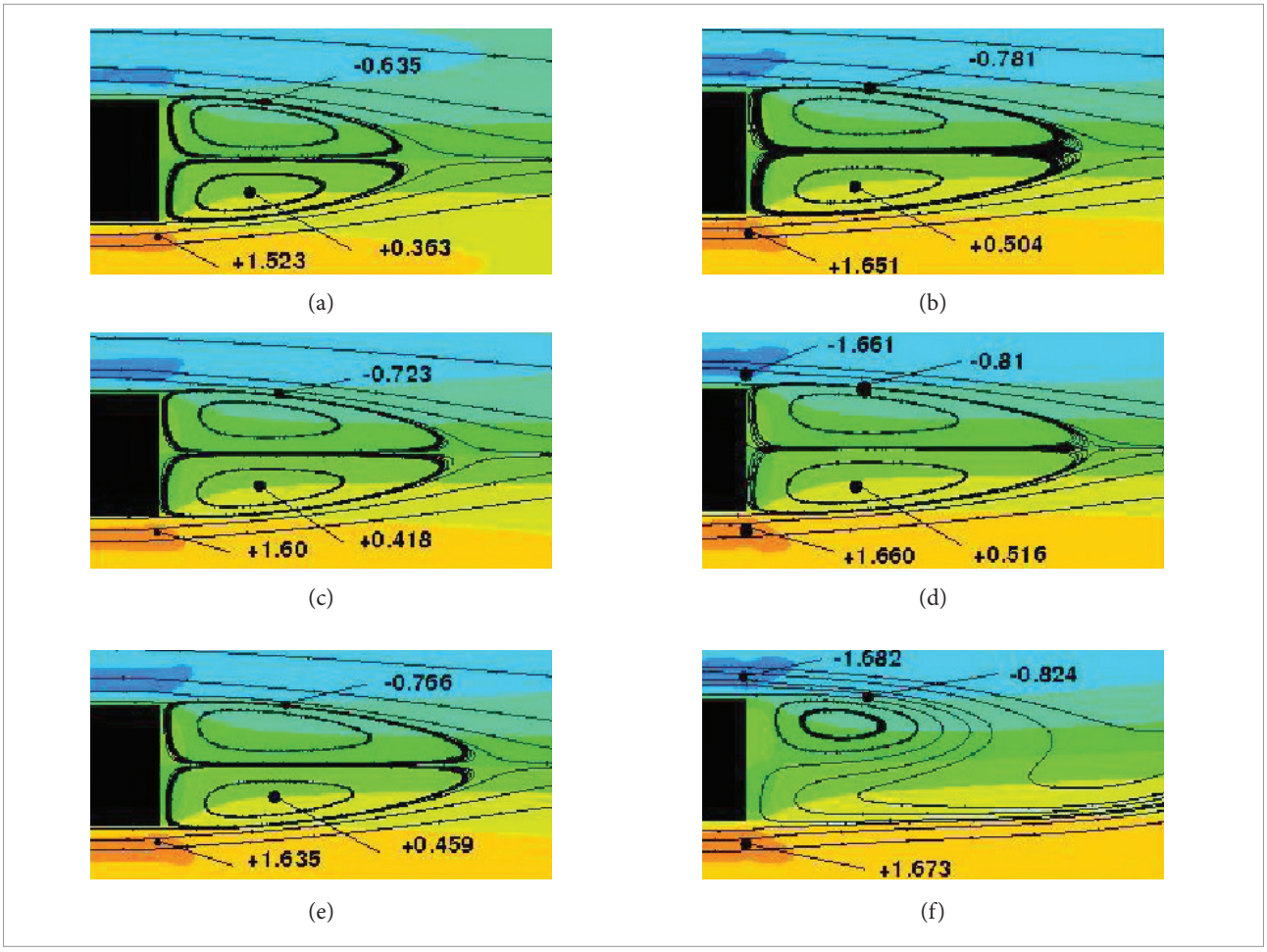

Figure 11. Evolution of the vorticity at the base region of the $AR = 14$ body, with varying Re. The numbers in each plot correspond to the dimensionless value of the vorticity. (a) $Re^h = 93$; (b) $Re^h = 95$; (c) $Re^h = 96$; (d) $Re^h = 97$; (e) $Re^h = 98$; (f) $Re^h_K = 100$.

CONCLUSIONS

The main goal of this research effort is to study the onset of shedding of the wake behind a blunt-trailing-edged body - an elongated cylinder with an elliptical front part. What motivated this study was the objective of obtaining, for this geometry, much of the same data (at least in quality) as there are for the circular cylinder. In this latter case, the reasons for the great interest of the engineering community are obvious, considering the myriad of applications of this geometrical form. On the other hand, the elongated body has a paramount advantage, in terms of easiness of analysis, because the points of separation are fixed. Therefore, with the elimination of the separation points excursions, some investigations and their consequent analyses are facilitated. We do believe that we have succeeded in our endeavor, and hope that the collection of results presented here will be of help for those individuals who are pursuing studies in this field. For example, the information contained in Fig. 5, and the studies carried out as a result of the boundary layers influence upon the stability of the great structures in the near wake of the body.

ACKNOWLEDGMENTS

The authors would like to acknowledge the support provided by the CNPq — *Conselho Nacional de Desenvolvimento Científico e Tecnológico* — (grant 303184/2007-8), and FAPESP — *Fundação de Amparo à Pesquisa do Estado de São Paulo* — (grant 2007/00305-5).

REFERENCES

Akselvoll, K. and Moin, P., 1996, "Large-eddy simulation of turbulent confined coannular jets", Journal of Fluid Mechanics, Vol. 315, pp. 387-411. doi:10.1017/S0022112096002479.

Barkley, D. and Henderson, R.D., 1996, "Three-Dimensional Floquet stability analysis of the wake of a circular cylinder" Journal of Fluid Mechanics, Vol. 322, pp. 215-241. doi:10.1017/S0022112096002777.

Bearman, P.W., 1965, "Investigation of the flow behind a two-dimensional model with a blunttrailing edge and fitted with splitter plates", Journal of Fluid Mechanics, Vol. 21, No 2, pp. 241-255. doi:10.1017/S0022112065000162.

Bearman, P.W., 1967, "The effect of base bleed on the flow behind a two-dimensional model with a blunt-trailing edge", Aero Quarterly, Vol. 18, pp. 207-214.

Bers, A., 1983, "Basic Plasma Physics I", In: Handbook of Plasma Physics (ed. M. N. Rosenbluth & R. Z. Sagdeev), Vol. 1, Chap. 3.2, North Holland.

Braza, M., Chassaing, P. and Ha Minh, H., 1986, "Numerical study and physical analysis of the pressure and velocity fields in the near wake of a circular cylinder", Journal of Fluid Mechanics, Vol. 165, pp. 79-130. doi: 10.1017/S0022112086003014.

Chomaz, J.M., Huerre, P. and Redekopp, L.G., 1988, "Bifurcations to local and global modes in spatially developing flows", Phys Rev Lett, Vol. 60, No 1, pp. 25-28. doi:10.1103/PhysRevLett.60.25.

Dauchy, C., Dussëk, J. and Fraunié, P., 1997, "Primary and secondary instabilities in the wake of a cylinder with free ends", Journal of Fluid Mechanics, Vol. 332, pp. 295-339.

Drazin, P.G. and Reid, W.H., 2004, "Hydrodynamic stability", 2nd Edition, Cambridge University Press, Cambridge, UK.

Dusëk, J., Fraunié, P. and Le Gal, P., 1994, "Local analysis of the onset of instability in shear flows", Phys Fluids, Vol. 6, No 1, pp. 172-186.doi: 10.1063/1.868080.

Fadlun, E.A., Verzicco, R., Orlandi, P. and Mohd-Yusof, J., 2000, "Combined immersed-boundary finite-difference methods for three-dimensional complex flow simulations", Journal of Computational Physics, Vol. 161, No 1, pp. 35-60. doi: 10.1006/jcph.2000.6484.

Goldstein, G., Handler, R. and Sirovich, L., 1993, "Modeling a no-slip flow boundary with an external force field", Journal of Computational Physics, Vol. 105, pp. 354-366. doi: 10.1006/jcph.1993.1081.

Huerre, P. and Monkewitz, P.A., 1985 "Absolute and convective instabilities in free shear layers" Journal of Fluid Mechanics, Vol. 159, pp. 151-168. doi:10.1017/S0022112085003147.

Jackson, C.P., 1987, "A finite-element study of the onset of vortex shedding in flow past variously shaped bodies", Journal of Fluid Mechanics, Vol. 182, pp. 23-45. doi: 10.1017/S0022112087002234.

Kravchenko, A.G. and Moin, P., 1997, "On the effect of numerical errors in large eddy simulations of turbulent flows", Journal of Computational Physics, Vol. 131, No 2, pp. 310-322. doi: 10.1006/jcph.1996.5597.

Laizet, S., Lamballais, E. and Vassilicos, J.C., 2009, "A numerical strategy to combine high-order schemes, complex geometry and parallel computing for high resolution DNS of fractal generated turbulence", Journal of Computer & Fluids. doi:10.1016/j.compfluid.2009.09.018.

Lardeau, S., Lamballais, E. and Bonnet, J.P., 2002, "Direct Numerical Simulation of a Jet Controlled by Fluid Injection", Journal of Turbulence, Vol. 3, No 1, pp. 002-011. doi: 10.1088/1468-5248/3/1/002.

Lamballais, E., 1996, « Simulation numériques de la turbulence dans un canal plan tournant », PhD Dissertation, Laboratoire Descoulements Gophysiques Et Industrielles, Institut National Polytechnique de Grenoble.

Lamballais, E. and Silvestrini, J.H., 2002, "Direct numerical simulation of interactions between a mixing layer and a wake around a cylinder", Journal of Turbulence, Vol. 3, pp. 028-036. doi:10.1088/1468-5248/3/1/028.

Lamballais, E., Silvestrini, J. and Laizet, S., 2008, "Direct Numerical Simulation of a Separation Bubble on a Rounded Finite-Width Leading Edge", International Journal of Heat and Fluid Flow, Vol. 29, No 3, pp. 612-625. doi:10.1016/j.ijheatfluidflow.2008.03.006.

Lele, S., 1992, "Compact finite difference schemes with spectral-like resolution", Journal of Computational Physics, Vol. 103, No 1, pp. 16-42. doi:10.1016/0021-9991(92)90324-R.

Mathis, C., Provansal, M. and Boyer, L., 1984, "The Bénard-von Kármán instability: an experimental study near the threshold", Journal de Physique – Lettres, Vol. 45, No 10, pp. 483-491. doi: 10.1051/jphyslet:01984004501004830O.

Monkewitz, P., 1988, "The absolute and convective nature of instability in two-dimensional wakes at low Reynolds numbers" Physics Fluids, Vol. 31, No 5, pp. 999. doi: 10.1063/1.866720.

Ortega, M.A., Girardi, R.M. and Silvestrini, J.H., 2012, "A numerical study of the wake behind a blunt-trailing-edged body. Part 2: the topology of the flow", International Journal for Numerical Methods in Fluids, Vol. 69, No 1, pp. 29-56. doi: 10.1002/fld.2533.

Park, H., Lee, D., Jeon, W.-P., Hahn, S., Kim, J., Kim, J., Choi, J. and Choi, H., 2006, "Drag reduction in flow over a two-dimensional bluff body with a blunt trailing edge using a new passive device" Journal of Fluid Mechanics, Vol. 563, pp. 389-414. doi:10.1017/S0022112006001364.

Provansal, M., Mathis, C. and Boyer, L., 1987, "Bénard-von Kármán instability: transient and forced regimes", Journal of Fluid Mechanics, Vol. 182, pp. 1-22. doi: 10.1017/S0022112087002222.

Ribeiro, P.A.R., 2002, "The control of the vortexes shedding mechanism in the wake of circular cylinders by means of numerical simulation", Master in Science Thesis, Federal University of Rio Grande do Sul, Porto Alegre, RS, Brazil (in Portuguese).

Rowe, A., Fry, A.L.A. and Montallebi, F., 2001, "Influence of boundary-Layer thickness on base pressure and vortex shedding frequency", AIAA Journal, Vol. 39, No 4, pp. 754-756. doi: 10.2514/2.1377.

Ryan, K., Thompson, M.C. and Hourigan, K., 2005, "Three-dimensional transition in the wake of bluff elongated cylinders", Journal of Fluid Mechanics, Vol. 538, pp. 1-29. doi:10.1017/S0022112005005082.

Saiki, E.M. and Biringen, S., 1996, "Numerical simulation of a cylinder in uniform flow: Application of a virtual boundary method", Journal of Computational Physics, Vol. 123, No 2, pp. 450-465. doi:10.1006/jcph.1996.0036.

Silvestrini, J.H. and Lamballais, E., 2004, "Direct numerical simulation of oblique vortex shedding from a cylinder in shear flow", International Journal of Heat and Fluid Flow, Vol. 25, No 3, pp. 461-470. doi: 10.1016/j.ijheatfluidflow.2004.02.013.

Sieverding, C.H. and Heinemann, H., 1990, "The influence of boundary layer state on vortex shedding from at plates and turbine cascades", Journal of Turbo-machinery, Vol. 112, No 2, pp. 181-187. doi:10.1115/1.2927631.

Schlichting, H., 1979, Boundary-Layer Theory. 7th ed. ,McGraw-Hill Series in Mechanical Engineering. New York.

Sumer, B.M. and Fredsøe, J., 1997, "Hydrodynamics around cylindrical structures", Advanced Series on Ocean Engineering, World Scientific Pub Co Inc, London, UK.

Triantafyllou, G.S., Triantafyllou, M.S. and Chryssostomidis, C., 1986, "On the formation of vortex streets behind stationary cylinders", Journal of Fluid Mechanics, Vol. 170, pp. 461-477. doi: 10.1017/S0022112086000976.

Vitola, M.A., 2006, "Onset of shedding of a circular cylinder in the presence of flat plate", PhD Dissertation, Federal University of Rio Grande do Sul, Porto Alegre, RS, Brazil (in Portuguese).

Yang, X. and Zebib, A., 1989, "Absolute and convective instability of a cylinder wake", Physics of Fluids A, Vol. 1, No 4, pp. 689. doi: 10.1063/1.857362.

Williamson, C.H.K., 1996, "Vortex dynamics in the cylinder wake", Annual Review of Fluid Mechanics, Vol. 28, pp. 477-539. doi: 10.1146/annurev.fl.28.010196.002401.